Journal of Computational Neuroscience 12, 147–163, 2002

Relation Between Potassium-Channel Kinetics and the Intrinsic Dynamics in Isolated Retinal Bipolar Cells

BU-QING MAO
Department of Neurology and Neuroscience, Weill Medical College of Cornell University, 1300 York Avenue, New York, NY 10021

PETER R. MACLEISH
Dyson Vision Research Institute, Department of Ophthalmology, Weill Medical College of Cornell University, 1300 York Avenue, New York, NY 10021 and Neuroscience Institute, Morehouse School of Medicine, 720 Westview Drive, S.W. Atlanta, GA 30310

JONATHAN D. VICTOR
Department of Neurology and Neuroscience, Weill Medical College of Cornell University, 1300 York Avenue, New York, NY 10021
jdvicto@med.cornell.edu

Received August 15, 2001; Revised March 6, 2002; Accepted March 22, 2002

Action Editor: Xiao-Jing Wang

Abstract. Characterization of the intrinsic dynamics of isolated retinal bipolar cells by a whole-cell patch-clamp technique combined with estimation of effective impulse responses across a range of mean injected currents reveals strikingly adaptive behavior. At resting potential, bipolar cells' effective impulse response is slow, high gain, and low pass. Depolarization speeds up response, decreases gain, and, in most cells, induces bandpass behavior.

This adaptive behavior involves two K^+ currents. The delayed-rectifier accounts for the observed gain reduction, speed increase, and bandpass behavior. The A-channel further shortens the impulse responses but suppresses bandpass features. Computer simulations of model neurons with a delayed-rectifier and varying A-channel conductances reveal that impulse responses largely reflect the flux of electrical charge through the two K^+ channels. The A-channel broadens the frequency response and preempts the action of the delayed-rectifier, thereby reducing the associated bandpass features. Admixtures of the two K^+ channels produce the observed variety of dynamics of retinal bipolar cells.

Keywords: delayed-rectifier, A-channel, impulse response, adaptive, bandpass

1. Introduction

K^+ channels in neurons serve diverse functions ranging from homeostasis to the regulation of firing frequency (Rudy, 1988). In sensory systems, K^+ channels play specific roles such as synaptic integration (Laurent, 1990), adaptation (Weckström et al., 1991), signal acceleration (Beech and Barnes, 1989), high-frequency enhancement (Attwell et al., 1982; Owen and Torre, 1983; Perlman et al., 1993), membrane resonance (Lewis and Hudspeth, 1983; Puil et al., 1988), and phase-locked activity (Reyes et al., 1994).

K^+ currents determine the intrinsic dynamics of retinal bipolar cells in tiger salamanders. Bipolar cells

respond to current inputs with adaptive dynamics that depend on the mean input currents (Mao et al., 1998). Depolarization of membranes reduces gain, increases the speed of response, and induces a shift from lowpass to bandpass behavior of the transfer function, typically associated with the emergence of an undershoot in the impulse response. The adaptive behavior also modifies the transfer functions of bipolar cells at low frequencies but not at high frequencies and bears strong similarities to changes in gain and dynamics observed in retinal neurons during light adaptation (Tranchina et al., 1984; Purpura et al., 1990).

This general picture of the intrinsic dynamics is complicated by the diversity in the kinetic types of K^+ currents. In isolated tiger salamander bipolar cells, this mixture typically includes sustained and transient components (Mao et al., 1998). The present study aims to determine the roles of two distinct K^+ channels, the delayed-rectifier and the A-channel, in shaping the bipolar cells' dynamic behavior. Bipolar cell dynamics was characterized by applying current stimuli with the profile of an *m*-sequence (Sutter, 1987; Victor, 1992; Mao et al., 1998) to measure the cells' effective impulse response. We combine these measurements with pharmacological dissection and computer simulation to explore how the delayed-rectifier and the A-channel interact to shape bipolar cells' dynamic features.

2. Methods

2.1. *Dissociation of Retina and Electrophysiological Recording*

Retinae of tiger salamanders (from Kons Scientific Co., Inc., Germantown, WI) were enzymatically dissociated (MacLeish et al., 1984) in a solution containing 10 units/ml papain (Worthington Biochemical Corp., Lakewood, NJ) and (in mM): 84 NaCl, 3 KCl, 25 $NaHCO_2$, 0.5 NaH_2PO_4, 1 Na pyruvate, 0.5 $CaCl_2$, 16 glucose, 2 d,l-cysteine HCl, and 0.02 phenol red, bubbled with a mixture of 95% O_2 and 5% CO_2. The retinae were digested for 30 to 45 minutes, rinsed, triturated, and plated onto coverslips treated with the antibody Sal-1 (MacLeish et al., 1983). The isolated cells were maintained for up to one week in 10°C in a medium containing (in mM): 108 NaCl, 3 KCl, 0.5 $MgCl_2$, 0.5 $MgSO_4$, 1 $NaHCO_3$, 0.5 NaH_2PO_4, 1 Na pyruvate, 0.1 choline Cl, 1.8 $CaCl_2$, 1 HEPES, 16 glucose, 0.02 phenol red, and 50 μg/ml bovine serum albumin. Osmolarity was adjusted to 240 mosM and pH to 7.2 to 7.4.

Whole-cell patch-clamp recordings were made typically within two days after retina dissociation using a List EPC-7 amplifier (set at 3 kHz) and PCLAMP6 software (Axon Instruments, Inc., Foster City, CA). Electrodes were pulled from borosilicate micropipettes (Drummond Scientific Company, Broomall, PA) on a BB-CH-PC puller (Mecanex S.A., Switzerland) and had a 1 μm tip opening and 5 to 15 MΩ resistance when filled with internal solution containing (in mM) 113 KCl, 0.05 EGTA, 1 ATP, 5 $MgCl_2$, and 10 HEPES, with osmolarity adjusted to 240 mosM and pH to 7.2. External solutions (A through E) are listed in Table 1, all with osmolarity 240 mosM and pH 7.4. Most of the experiments were performed under solution A. Solution B has 35 mM choline Cl substituting equal-osmolar NaCl and was used as control solution in pharmacological studies in which TEA and/or 4-AP was added (solutions C, D, and E) to replace equal-osmolar choline Cl.

2.2. *Characterization of Dynamics Using the M-Sequence Method*

The dynamics of bipolar cells were characterized under current-clamp by their effective impulse responses to injected currents with means ranging from −25 pA to 100 pA. Superimposed on each mean current were fluctuations whose temporal profile was determined

Table 1. External solutions.

mM	NaCl	KCl	Choline Cl	$CaCl_2$	$MgCl_2$	Glucose	HEPES	Phenol red	TEA Cl	4-AP HCl
A	108	3		2.5	1	16	5	0.02		
B	70	3	35	2.5	1	16	5	0.02		
C	70	3	17	2.5	1	16	5	0.02	20	
D	70	3	10	2.5	1	16	5	0.02	20	6
E	70	3	30	2.5	1	16	5	0.02		3

by a binary m-sequence (Sutter, 1987; Victor, 1992). The set of effective impulse responses captures the cells' response to incremental changes in input current (which contain a broad spectrum of frequency components) at each depolarization level. Details of the m-sequence method can be found in Sutter (1987), Victor (1992), and Mao et al. (1998). Briefly, a binary m-sequence of order M is a cyclic binary sequence $\{m_1, m_2, \ldots, m_N\}$ of length $N = 2^M - 1$ whose autocorrelation for all nonzero time lags is very nearly zero. In the present study, we used $M = 11$ and $N = 2047$, and the binary sequence $\{m_1, m_2, \ldots, m_N\}$ of -1's and 1's was translated into a time-varying current $S(t) = \mu + \alpha m_i$, $iT_s \le t \le (i+1)T_s$, in which α (in pA) is the current amplitude scale factor and T_s (in ms) is the time interval. μ (in pA) is the mean current and determines whether the cell is depolarized ($\mu > 0$), hyperpolarized ($\mu < 0$), or held at resting potential ($\mu = 0$). For each μ, the cell's effective impulse response, $h(t)$, was estimated by a cross-correlation between the m-sequence current input and the cell's membrane voltage response (in mV). The relationship among the discretized impulse response $h_n = h(nT_s)$, the m-sequence current $S_n = S(nT_s)$, and the membrane-voltage response $R_n = R(nT_s)$, is determined by a cross-correlation following correction for a DC offset (Mao et al., 1998):

$$\frac{N+1}{N} h_k - \frac{1}{N} \sum_{i=0}^{N-1} h_i = \frac{1}{\alpha^2 T_s} \frac{1}{N} \sum_{n=0}^{N-1} R_n S_{n-k}, \quad (0 \le k < N),$$

in which subscripts on S are interpreted mod N.

The impulse response $h(t)$ has units of mV/(pA · ms) or mV/fCoulomb. For each impulse response, we define DC gain as the limit of amplitude of transfer function (the Fourier transform of the impulse response) as frequency approaches zero. From this definition, DC gain can be calculated as the integral of impulse response with respect to time, or, equivalently, the area under the impulse response curve. The initial decay of each impulse response was also fitted with a single exponential function. For details, see Mao et al. (1998) and Mao (1997). The time constant for each impulse response was obtained directly from the fitted exponential function. From the estimated impulse responses of each cell, we calculated a bandpass index (details in Results) to measure the effect of A-channel and delayed-rectifier on intrinsic dynamics.

2.3. *Experimental Implementation of the M-Sequence Method*

The choices of amplitude scale factor α and time interval T_s were based on the following considerations. Since both DC gain and time constant (or speed) of a bipolar cell's impulse response depend strongly on the mean current (Mao et al., 1998), a series of m-sequence currents with different mean levels (typically, -25, -3, 0, 3, 7, 15, 25, 50, 75, and 100 pA) were needed to capture the range of a bipolar cell's dynamic behavior. For each mean current, the time interval T_s of the m-sequence was chosen empirically to accommodate the speed of the membrane-voltage response customarily associated with that mean current based on pilot experiments. T_s ranged from 0.05 ms (for mean currents >50 pA, at which responses were fast) to 1.5 ms (for mean currents around 0 pA, at which responses were slow). The T_s for mean current -25 pA was determined during experiment, depending on whether the bipolar cell under study had a significant h-current. If it did, T_s was chosen be 0.1 ms, to accommodate the speed of response at that mean current; otherwise, T_s was chosen to be the same as that for 0 pA. The amplitude α for the m-sequence fluctuation was chosen according to two constraints. To maintain a sufficient signal-to-noise ratio, α could not be too small. However, with increasing α membrane voltage deviation would increase, and consequently the bipolar cells could deviate from linear behavior. We chose α such that voltage deviation was around 15 mV. Since linearity was important for some of our characterizations of the bipolar cells' dynamics (such as impulse response and transfer function), it was tested in pilot experiments. In the pilot experiments, the set of m-sequence currents were delivered in a random order, with high and low mean current levels interleaved, to prevent biases that might result from slow changes in the preparation. Once the order was decided, it was used in all experiments. Pilot experiments showed that, with this set of stimuli, the bipolar cell indeed behaved in an approximately linear manner if mean current is held constant. Specifically, at any given level of mean current, increasing or decreasing the current amplitude α by a factor of 10, or increasing or decreasing the time interval T_s by a factor of 3, did not change the estimated impulse response. Data acquired from

m-sequence experiments were analyzed with in-house software.

2.4. Characterization of Voltage-Dependent K^+ Currents

Voltage-activated currents of bipolar cells were obtained by standard voltage-clamp techniques and analyzed with PCLAMP6 software (Axon Instruments, Inc., Foster City, CA). Delayed-rectifier and A-channel currents were isolated by the application of channel blockers TEA or 4-AP or both (Solutions C, D, and E) and analyzed by a current subtraction protocol in which pairs of current recordings corresponding to the same set of voltage commands were subtracted to obtain the current component blocked by the specific channel blockers. Powers of exponential curves were fitted to voltage-clamped currents using PCLAMP6 software. For the delayed-rectifier channel, a Hodgkin-Huxley model of order 2 was found to best fit its activation time course. Amplitudes and time constants thus obtained were subsequently converted to standard channel parameters such as α and β for channel kinetics as listed in the footnotes for Table 3. For the A-current, only the inactivation time course was fitted; the best fit was with an exponential of power 1. The amplitude of the rising phase was fitted to the function in Table 3. Since the speed of A-current precluded a quantitative fit, a single exponential of time constant 1 to 4 msec (the precise value did not affect the simulations) was used for activation kinetics.

2.5. Computer Simulations

The relationship between the A-channel and delayed-rectifier and the bipolar cells' dynamic features was explored by computer simulations using Runge-Kutta algorithms (Press et al., 1992). Aspects examined included families of impulse responses, electrical charge flows, bandpass indices, membrane potentials, gains, and transfer functions. Parameters used for the model neuron are listed in Table 3. The geometric characteristics of isolated bipolar cells allows a model with all elements lumped and in parallel with each other, under the assumption of space-clamping and uniform membrane distribution of all conductances. Values of conductances and capacitance chosen are from this and our previous studies (Mao et al., 1998), as specified later in Results section.

3. Results

3.1. Dynamics of Bipolar Cells Are Correlated with the Kinetics of Their Outward Currents

Isolated bipolar cells were identified by the characteristic Landolt club, an enlargement of the primary dendrite from an initially narrower segment of the dendrite (Hare et al., 1986; Mao et al., 1998). The axons of bipolar cells were usually lost in the dissociation process. Typical dynamic features of bipolar cells under current clamp are illustrated in recordings of two cells shown in Figs. 1A and 2A: The impulse responses are relatively slow near resting potential but become much faster with more depolarizing mean currents. DC gain and time constant are maximal at resting potential (4.95 ± 2.05 mV/pA, SD, $n = 52$, for DC gain, and 99.7 ± 52.1 ms, SD, $n = 52$, for time constant, at resting potential -37.6 ± 14.4 mV, SD, $n = 101$; Mao et al., 1998), but are sharply reduced by depolarization (typically by approximately two orders of magnitude at mean current 100 pA, for both DC gain and time constant). In many cells, an undershoot appears in the impulse responses for depolarizing mean currents >15 pA (Fig. 1A). An undershoot in the impulse response is typically associated with a bandpass transfer function. Indeed, families of transfer functions of these cells show a change from high-gain, low-pass behavior at resting potential to low-gain, bandpass behavior with progressive depolarization (Mao et al., 1998). In other cells, however, impulse responses contain virtually no undershoot (Fig. 2A), even though other dynamic features, such as the acceleration of impulse response and the reduction of gain, are as evident as in Fig. 1A. One consequence of an undershoot in the impulse response is that it predicts an overshoot (or transient) in the cells' voltage response to the more conventional current steps (at the same membrane potential as that for the impulse response), since the step-response of a linear system can be obtained by integrating its impulse-response with respect to time.

The impulse responses for depolarizing mean currents are plotted on a semi-logarithmic scale in the inset of Figs. 1A and 2A. On such a plot, a simple exponential decline would appear as a straight line. Thus, the downward bend (inset Fig. 1A) indicates that the return to zero of the impulse responses is accelerated,

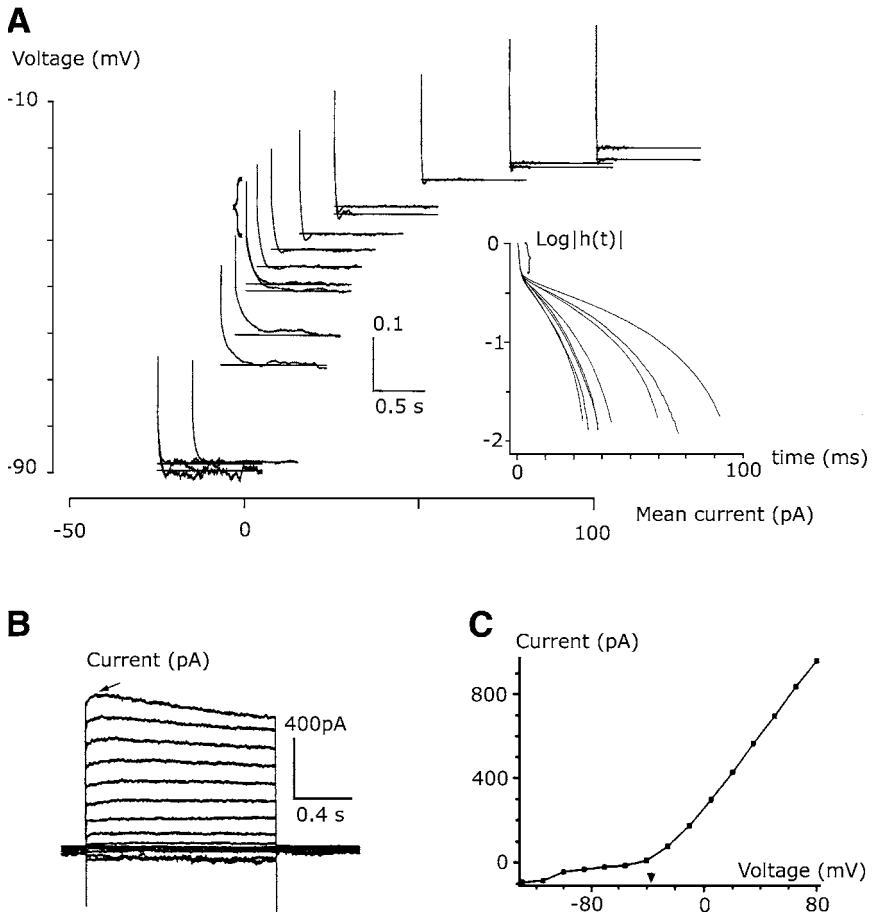

Figure 1. Bipolar cell recording #1 (from Group A). Recordings in solution A. **A:** Impulse responses (as functions of time) plotted in the (I, V) plane. The placement of the origin ($t = 0$) of each impulse response indicates mean current applied I (abscissa) and mean voltage response V (ordinate). The scale bar for impulse response amplitude has units mV/(pA · ms). The spikelike segment at $t = 0$ (one example marked by the bracket) in each impulse response reflects the series resistance of the electrode. Note the presence of undershoots at depolarizing mean currents. The bandpass index (see text) is 0.46. *Inset*: Semilogarithmic plots of declining phases (down to 1% of peak) of the impulse responses for depolarizing mean currents (7, 25, 35, 50, 75 pA). The more rapidly declining impulse-response curves correspond to the more depolarizing mean currents. The spikelike segment at $t = 0$ is more readily seen in the semilogarithmic plots (marked by the bracket). All the curves are concave downward, which indicates that their declining phase is more accelerated than an exponential decline fitted to the initial decay. **B:** Voltage-dependent currents of this cell have delayed-rectifier kinetics (marked by an arrow). Applied voltages are −140 to +80 mV, in 15 mV increments. **C:** I-V curve, derived from steady-state currents in panel B, shows activation at ca. −35 mV. The solid triangle indicates the voltage at which outward currents begin to activate.

presumably by voltage-dependent conductance activated at the depolarized membrane potentials.

Under voltage-clamp conditions, all bipolar cells contain an outward current activated at > -30 mV (Fig. 1B and C and Fig. 2B and C). The main component of the outward current is of the delayed-rectifier type (arrow in Fig. 1B), nearly sustained during the voltage pulse (ca. 1.3 sec). This component is found in all bipolar cells. A transient A-channel component is also seen in many cells (arrow in Fig. 2B) but not in all (e.g., Fig. 1B).

We next correlated the kinetics of the outward currents obtained by voltage steps (i.e., delayed-rectifier only versus delayed-rectifier *and* A-channel types) with response dynamics (i.e., the characteristics of how the impulse response depended on mean currents) across bipolar cells. Sixty recordings with a sufficiently complete family of step responses and impulse responses were examined for the presence of the A-channel. An A-channel current was indicated by a notch (arrow in Fig. 2B) in the outward current at the onset of each voltage pulse, which signifies the fast

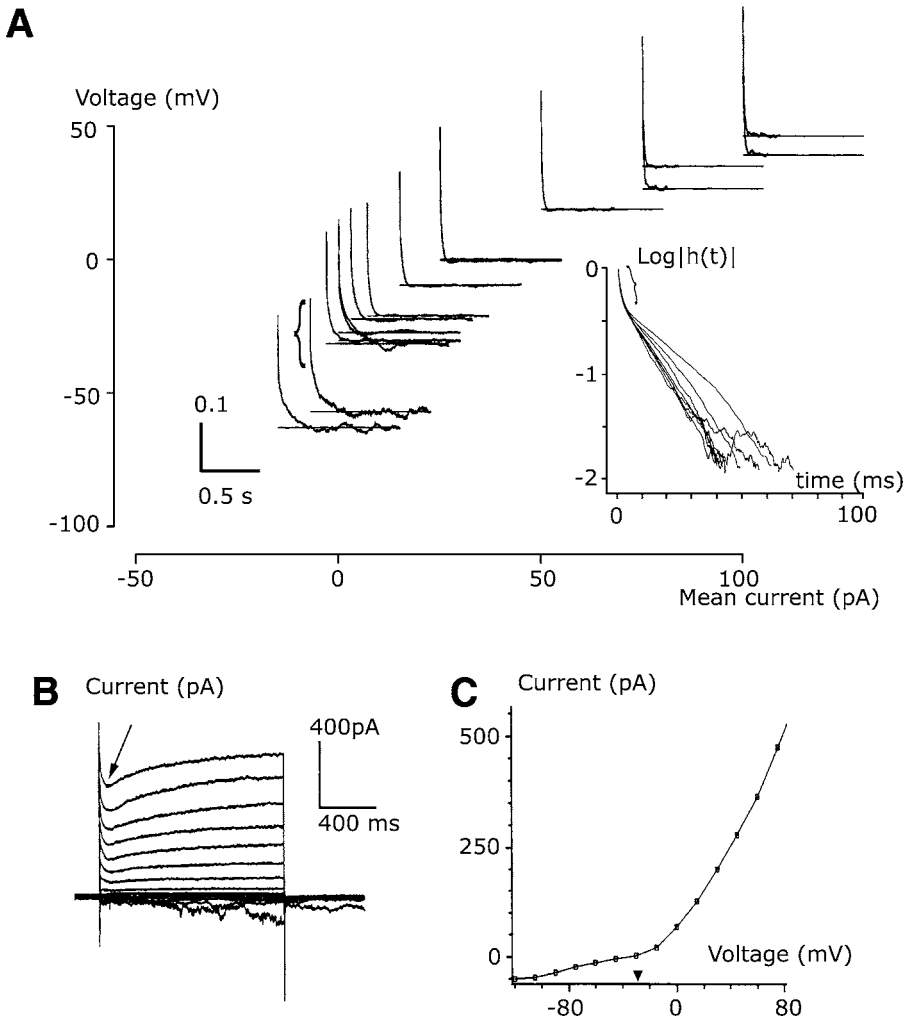

Figure 2. Bipolar cell recording #2 (from Group C). Recordings in solution A; plotting conventions as in Fig. 1. **A:** Depolarization did not result in undershoots in the impulse responses, despite their more rapid decline. The scale bar for impulse response amplitude has units mV/(pA · ms). The bracket indicates an example of the spike-like initial segment, reflecting series resistance of electrode. The bandpass index (see text) is 0.13. *Inset*: On a semilogarithmic scale, the decay of impulse responses for depolarizing mean currents (15, 25, 50, 75, 100 pA) did not show as much a delay as that in Fig.1A inset. The bracket indicates the spike-like segment. **B:** Activation of outward currents, which contain an A-channel-like component (arrow) in addition to a sustained delayed-rectifier component. Applied voltages are −120 to +75 mV, in 15 mV increments. **C:** I-V curve, derived from steady-state currents in panel B, shows activation at ca. −30 mV (solid triangle).

inactivation of this transient current before a slower (i.e., delayed-rectifier type) current reaches a steady-state. Twenty-two recordings (out of 60) had no A-channel component, and their impulse responses all contained an undershoot. Thirty-eight recordings (out of 60) had the A-channel component. Of these, 15 contained an undershoot in the impulse responses under depolarizing conditions, but 23 did not. Thus, the 60 recordings fall into three qualitative groups, designated as A, B, and C in Table 2. These results suggest that delayed-rectifier suffices to cause an undershoot (Group A), while the A-channel is not necessary. Indeed, the A-channel even appears to prevent the undershoot in some cases (Group C).

To confirm these results and to quantify the undershoots, we extracted a "bandpass index" for each of the 60 recordings as follows: (1) Two areas under each impulse-response curve were calculated: area p (from time zero to the first zero-crossing point) and area q (between the first and the second zero-crossing point,

Table 2. The relation between the A-channel-like current and features of the impulse response.

	A	*	B	C
Presence of A-channel	No	No	Yes	Yes
Presence of undershoot	Yes	No	Yes	No
Number of cells	22	0	15	23
Bandpass index	0.534 ± 0.149 (SD, $n = 32$)**		0.417 ± 0.132 (SD, $n = 23$)**	0.141 ± 0.138 (SD, $n = 29$)**

*Column 2 has no label, since no cells were observed with the characteristics corresponding to this column.
**Numbers (n) for statistics are larger than the number of cells since for many cells, two sets of impulse responses were obtained.

or, from the first zero-crossing point to the end of the measured impulse response if no other zero-crossing is present). (2) An index, $2q/(p+q)$, was calculated for each impulse-response curve. This index is 0 if the impulse response contains no undershoot ($q = 0$) and is 1 if the impulse response contains an undershoot that is sufficiently deep and/or lasts sufficiently long to reduce DC gain to 0 ($q = p$). Intermediate values of the index express the fractional reduction of the DC gain by the undershoot. (3) For each recording, the indices for all depolarizing currents >15 pA were averaged. Indices at lower mean currents were excluded from the average since this is the range of mean currents at which the undershoot is typically not manifest, and including them would just have added noise to the overall index. We also calculate a bandpass index for *each impulse response* from computer simulation, in which case step 3 was omitted.

The bandpass index calculated for recordings in Fig. 1 (from Group A) was 0.46 and that in Fig. 2 (from group C) was 0.13. Mean bandpass indices for recordings of group A, B, and C (Table 2) are 0.534 ± 0.149 (SD, $n = 32$), 0.417 ± 0.132 (SD, $n = 23$), 0.141 ± 0.138 (SD, $n = 29$), respectively. The differences between bandpass indices are significant: t-test $p < 0.001$ (A vs. B), $p < 10^{-9}$ (B vs. C), $p < 10^{-15}$ (A vs. C). Group A cells contain only the delayed-rectifier and not A-channel current, and this group has the highest bandpass index. Group B and C cells contain an A-channel current and their bandpass indices are significantly less than that of Group A cells. Thus, bandpass index measurements confirm that the delayed-rectifier causes bandpass behavior, while A-current tends to reduce bandpass behavior. Thus we detect a link between the delayed-rectifier and undershoot and a link between the A-current and the *absence* of undershoot. We later demonstrate how blocking the A-channel enhances and how increasing the A-channel conductance removes, bandpass features of bipolar cells.

3.2. *Inactivation of the Outward Currents*

We investigated whether the K^+ channel in the tiger salamander bipolar cells inactivates and, if so, how inactivation affects gain and dynamics. Evidence for voltage-dependent inactivation was seen in all of the bipolar cells in which such evidence was sought ($n = 20$). As Fig. 3A shows, we measured outward currents in response to a voltage pulse preceded by various depolarizing prepulses. Voltage-dependent inactivation is evident by the progressive decrease of the current responses for increasingly depolarizing prepulses. The channel does not need to open to inactivate: even for prepulses that did not activate a current (e.g., in the -100 to -60 mV range), the currents elicited by the test pulse still depend strongly on the level of the prepulses. The inactivation had a low threshold: in a majority of cells, the inactivation I-V curve (Fig. 3B) had a half-maximum at a voltage <-70 mV. Thus, at resting potential (ca. -37 mV), a high proportion of K^+ channels must be inactivated. In spite of this, the fraction of potassium conductance that is not inactivated at resting potential, though small, must be sufficient to produce changes in intrinsic gain and dynamics that we observed (see below) (Mao et al., 1998). We estimated the effective conductance of this available portion (not inactivated) of K^+ channels from impulse responses under extreme depolarizing conditions (e.g., at 75 pA or 100 pA), on the assumption that at these depolarization levels (ca. -20 mV), the bipolar cells' behavior is predominantly determined by this conductance. DC gain under such conditions is typically 0.35 GΩ, equivalent to a conductance of 2.9 nS. The leakage conductance (estimated from DC gain at resting potential) (Mao et al., 1998)

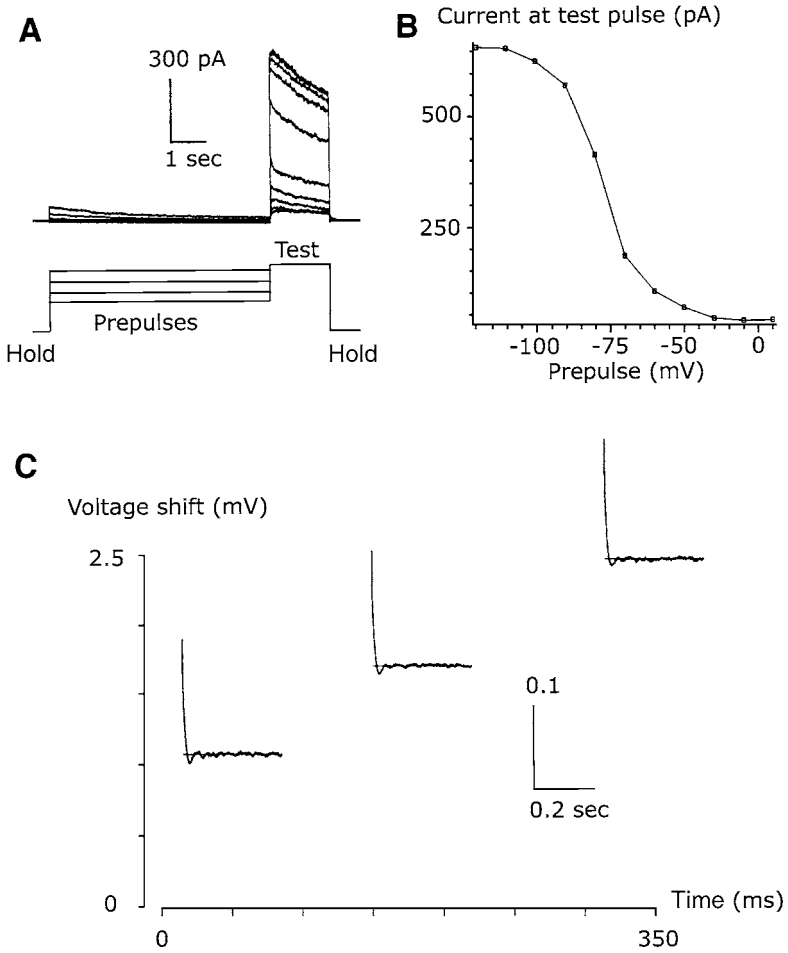

Figure 3. K^+-current inactivation and dynamics. **A:** Current responses to a test pulse (−10 mV, 1.5 sec) preceded by a range of prepulses (−120 to 10 mV, in 10 mV increments, 6 sec duration). Prepulses and test pulses are flanked by holding voltages of −70 mV, as diagrammed. K^+ current undergoes voltage-dependent inactivation: the lower the prepulse voltage, the larger the outward current elicited by the test pulse. **B:** Steady-state inactivation curve (current elicited by test pulse versus prepulse voltage) derived from panel A shows a half-maximum at ca. −73 mV. **C:** Impulse responses were estimated from twelve 2047-sample segments with different starting points on the voltage response to 2.5 cycles (5000 samples) of an *m*-sequence current with a mean of 100 pA. Three of the 12 impulse responses (including the first and twelfth) are plotted in the (V, t) plane: V is membrane voltage, and t is the time of the starting point of each segment on the voltage response. The vertical position of the three impulse responses indicates a depolarizing membrane voltage shift over time.

is typically 0.2 nS. Thus, the available K^+ conductance (i.e., the fraction of K^+ conductance that is not inactivated at resting potential) is at least an order of magnitude larger than the leakage conductances (nonspecific and voltage-independent K^+) and should contribute significantly to the cell's behavior.

How does voltage-dependent inactivation of K^+ conductance affect dynamics? We obtained impulse responses from segments starting from different points along the 5000-sample experimental record of voltage responses to the *m*-sequence input current. (The 5000-sample record contained 2.5 cycles of the response to the *m*-sequence, and thus estimates of impulse responses could be obtained from multiple subsections of the record.) Figure 3C shows an appreciable shift (1.5 mV) in membrane voltage over a 0.35 sec current injection with mean 100 pA (similarly for 50 and 75 pA), signifying a progressive inactivation of the K^+ conductance. However, throughout the recording, the impulse-response curves have similar shapes. Thus, the time course of inactivation does not affect bipolar cells' gain and dynamics.

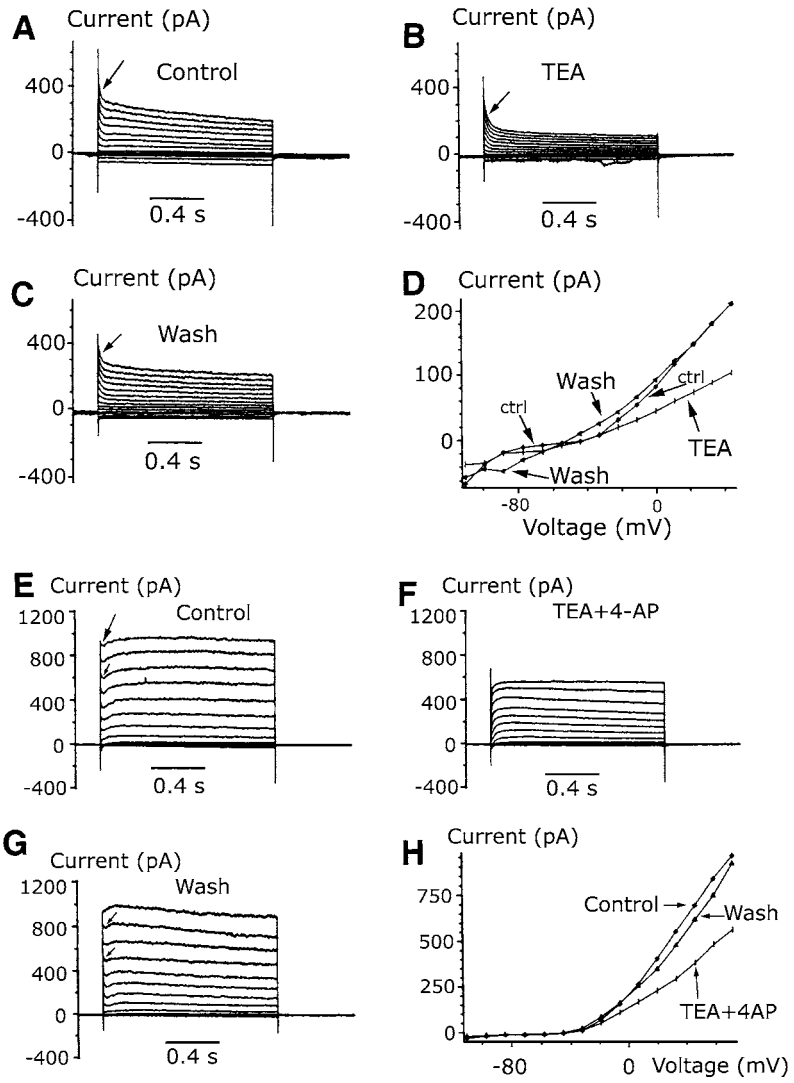

Figure 4. TEA and 4-AP block different kinetic components of outward currents. **A–D:** Voltage-clamp recordings demonstrating reversible reduction in outward currents by TEA. Voltage-dependent currents were obtained in external solution B (panel **A**) followed by exchange to solution C that contains 20 mM TEA (panel **B**), then back to solution B (panel **C**). Note that an early fast and transient component is resistant to TEA (arrows in panels A, B, and C). **D:** I-V curves derived from panels A–C. **E–H:** A similar experiment but in solutions D (20 mM TEA and 6 mM 4-AP) and B. The sustained component of the outward currents were reversibly depressed, presumably by TEA. Moreover, the fast transient component (at the onset of voltage pulses, indicated by the arrows in panels E and G) was also reversibly blocked (panel F), presumably by 4-AP. **H:** I-V curves derived from panels E–G.

3.3. Roles of the Delayed-Rectifier and A-Channel for Intrinsic Dynamics

The outward K^+ current in retinal bipolar cells is largely voltage-dependent, although it may contain a Ca^{++}-dependent component (Tessier-Lavigne et al., 1988). The outward current in our study did not have an N-shaped current-voltage relation, such as that observed in Kaneko and Tachibana (1985), which would have suggested a Ca^{++}-dependent component. Moreover, bipolar cells' adaptive behavior persists in 2.5 mM Co^{++} ($n = 5$), which is expected to block Ca^{++} entry. Therefore, Ca^{++} entry does not appear to be essential for the observed intrinsic dynamics.

In solutions with the K^+-channel blocker TEA (Hille 1967), the sustained delayed-rectifier component was depressed, but the transient A-channel component was unaffected (Fig. 4A–D; note arrows in panels A, B,

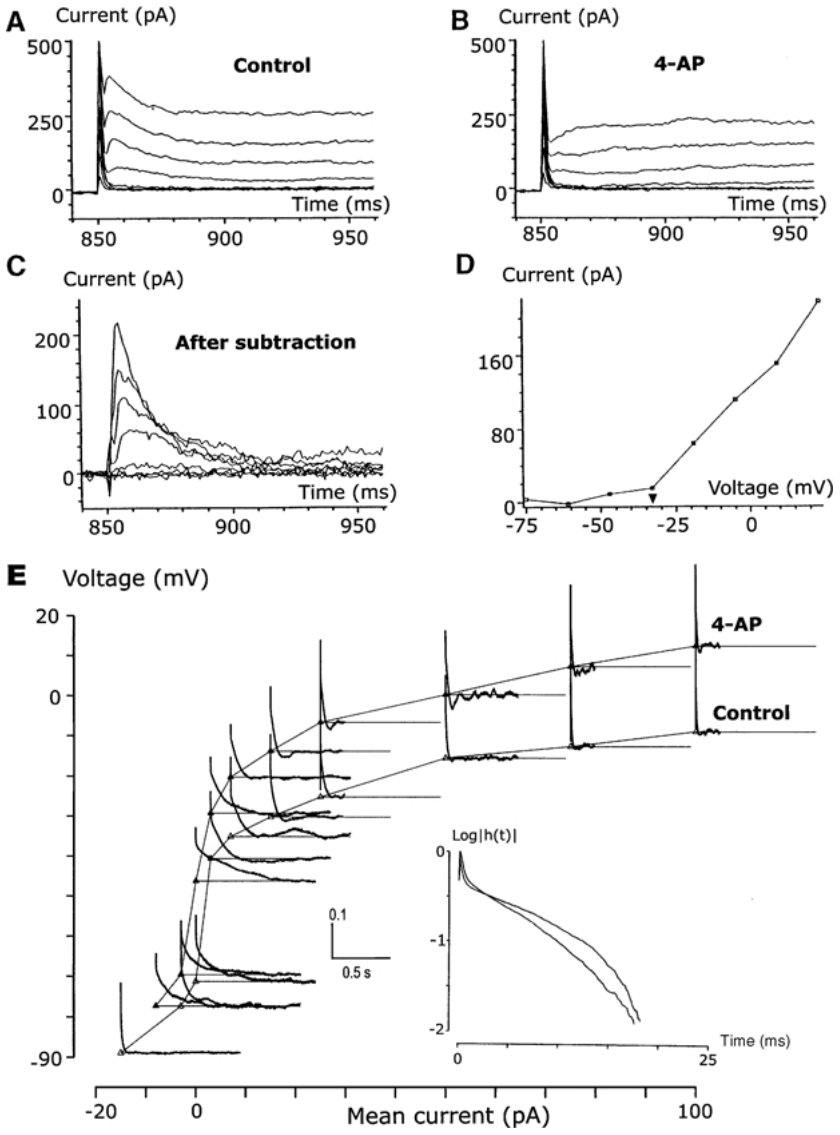

Figure 5. The 4-AP-sensitive current and impulse response. **A:** The outward current has an A-channel component in external solution B (without 4-AP). **B:** This A-channel component is eliminated when the medium is changed to solution E (3 mM 4-AP). The set of voltage commands is the same as that in panel A. **C:** Current subtraction (currents in panel A minus currents in panel B) reveals a fast-activating and transient A-channel current. **D:** I-V curve (from currents in panel C) indicates that this 4-AP-sensitive current (sampled at its peak) activates near −33 mV (solid triangle). **E:** Impulse responses of a bipolar cell perfused in solution B (without 4-AP) and solution E (3 mM 4-AP); plotting conventions same as in Figs. 1A and 2A. The scale bar for impulse response amplitude has units mV/(pA · ms). In the presence of 4-AP, undershoots are deeper and slower (the upper set of impulse response curves). *Inset*: Impulse responses for mean current 100 pA in solutions E (3 mM 4-AP) and B (control), plotted on a semilogarithmic scale. With 4-AP, there appears to be a delay before the beginning of acceleration in the decline of the impulse response.

and C). TEA (solution C of Table 1) reduced the steady-state current (for a holding voltage of 44 mV) to 48% ± 11% (SD, $n = 3$) of control. The A-channel is blocked by 4-AP (Thompson, 1977; Meves and Pichon, 1977; Yeh et al., 1976). Thus solution D, which contains both 4-AP and TEA, not only reduced the outward current but also eliminated the fast transient A-channel component (Fig. 4E–H; note arrows in E and G but not in F).

The A-channel component activates quickly (time-to-peak typically <5 ms) and deactivation completes within 50 ms (Fig. 5A–C). The voltage range of its activation, >−33 mV (solid triangle, Fig. 5D), is similar

to that of the delayed-rectifier component (cf. Figs. 1C and 2C). Because the ranges of activation of the two channels overlap, they can interact substantially.

The nature of this interaction is illustrated by comparing impulse responses measured from cells perfused, alternately, in solutions with and without 4-AP. Figure 5E shows two (of three) interleaved sets of impulse responses thus obtained. With 3 mM 4-AP (solution E), undershoots are pronounced, prolonged and, in some recordings, followed by oscillatory wavelets. In contrast, impulse responses obtained in control solution B have shallow and brief undershoots (if at all). The two sets of impulse responses also differ in the slope of the declining phase (Fig. 5E inset). With 4-AP, the slope bends downward after a delay, revealing the sluggish nature of the remaining delayed-rectifier component. Without 4-AP, the slope is steeper, i.e., the decline is faster, signifying the action of the 4-AP-sensitive current. These results suggest that the A-channel component speeds up impulse responses of bipolar cells, but that the A-channel is not necessary for the shift of dynamics from lowpass (no undershoot) to bandpass (undershoot) behavior. Indeed, A-channel tends to eliminate this aspect of bipolar cells' dynamics, as we illustrate next.

3.4. *Interaction Between the A-Channel and the Delayed-Rectifier*

We explored the interaction between the A-channel and the delayed-rectifier conductances by computer simulations on a single-compartment model neuron that contains a delayed-rectifier, an A-channel, a voltage-independent K^+ conductance, and a nonspecific leakage conductance (Table 3). The functional form of the model for the delayed rectifier channel was modified from Hodgkin and Huxley (1952), and that for the A-channel was modified from Connor et al. (1977). The individual parameter values (a_k, b_k, c_k and d_k) were adjusted to fit typical datasets. Key characteristics of the channels are as follows. For the delayed-rectifier, activation begins at ca. −35 mV, with half-maximal activation at ca. 0 mV. For the A-channel, activation begins at ca. −40 mV, with half-maximal activation at ca. 0 mV and half-maximal inactivation at ca. −20 mV. Across the voltage range −50 to 0 mV, the time constant for the activation of the delayed rectifier ranges from 55 to 25 msec. The time constant τ_A for A-channel activation was presumed to be extremely fast, and we set it at 1 ms (we also used up to 4 msec, and the results are similar). We used a delayed-rectifier conductance G_{DR} of 5 nS and A-channel conductances G_A of 0, 1, 2, 4, 8, 15, 25 nS. The K^+-specific leakage conductance G_{kleak} is 0.1 nS and the nonspecific leakage conductance G_{ns} 0.1 nS, in agreement with the maximum gain of 4.95 ± 2.1 mV/pA, $n = 52$, or, equivalently, 0.2 nS, at resting potential. The capacitance of the model neuron is 10 pF (based on 10.2±3.6 pF, $n = 81$) (Mao et al., 1998).

The interaction between the A-channel and the delayed-rectifier was studied by varying G_A (0, 1, 2, 4, 8, 15, 25 nS) while keeping G_{DR} constant (5 nS).

Table 3. Parameters of a model neuron for computer simulations.

Element	Value	Reversal potential	Kinetics
Membrane capacitance	$C_m = 10$ pF		
Nonspecific leakage conductance	$G_{ns} = 0.10$ nS	0 mV	Ohmic
Voltage-independent K^+ conductance	$G_{Kleak} = 0.10$ nS	−90 mV	Ohmic
Delayed-rectifier conductance	$G_{DR} = 5$ nS	−90 mV	*
A-channel conductance	$G_A = 0, 1, 2, 4, 8, 15, 25$ nS	−90 mV	**

*Kinetic model of the delayed-rectifier (modified from Hodgkin and Huxley, 1952).
Activation: $\alpha = a_1(V - b_1)/\{1 - \exp[(b_1 - V)/c_1]\}$, $a_1 = 0.003$ ms^{-1}, $b_1 = -3$ mV, $c_1 = 8$ mV.
$\beta = a_2(b_2 - V)/\{1 - \exp[(V - b_2)/c_2]\}$, $a_2 = 0.0002$ ms^{-1}, $b_2 = -30$ mV, $c_2 = 80$ mV.
$n_\infty = \alpha/(\alpha + \beta)$, $\tau = 1/(\alpha + \beta)$, $g = G_{DR} \cdot n^2$.
** Kinetic model of the A-channel (modified from Connor et al., 1977).
Activation: $A_\infty = 1/[1 + \exp((V + a_1)/b_1)]$, $a_1 = -20$ mV, $b_1 = -8$ mV; $\tau_A = 1$ to 4 ms.
Deactivation: $B_\infty = 1/[1 + \exp((V + a_3)/b_3)]$, $a_3 = -30$ mV, $b_3 = 14$ mV.
$\tau_B = a_4 + b_4/\{1 + \exp[(V + c_4)/d_4]\}$, $a_4 = 0.2$ ms, $b_4 = 0.8$ ms, $c_4 = 40$ mV, $d_4 = 16$ mV.
$g = G_A \cdot A \cdot B$.

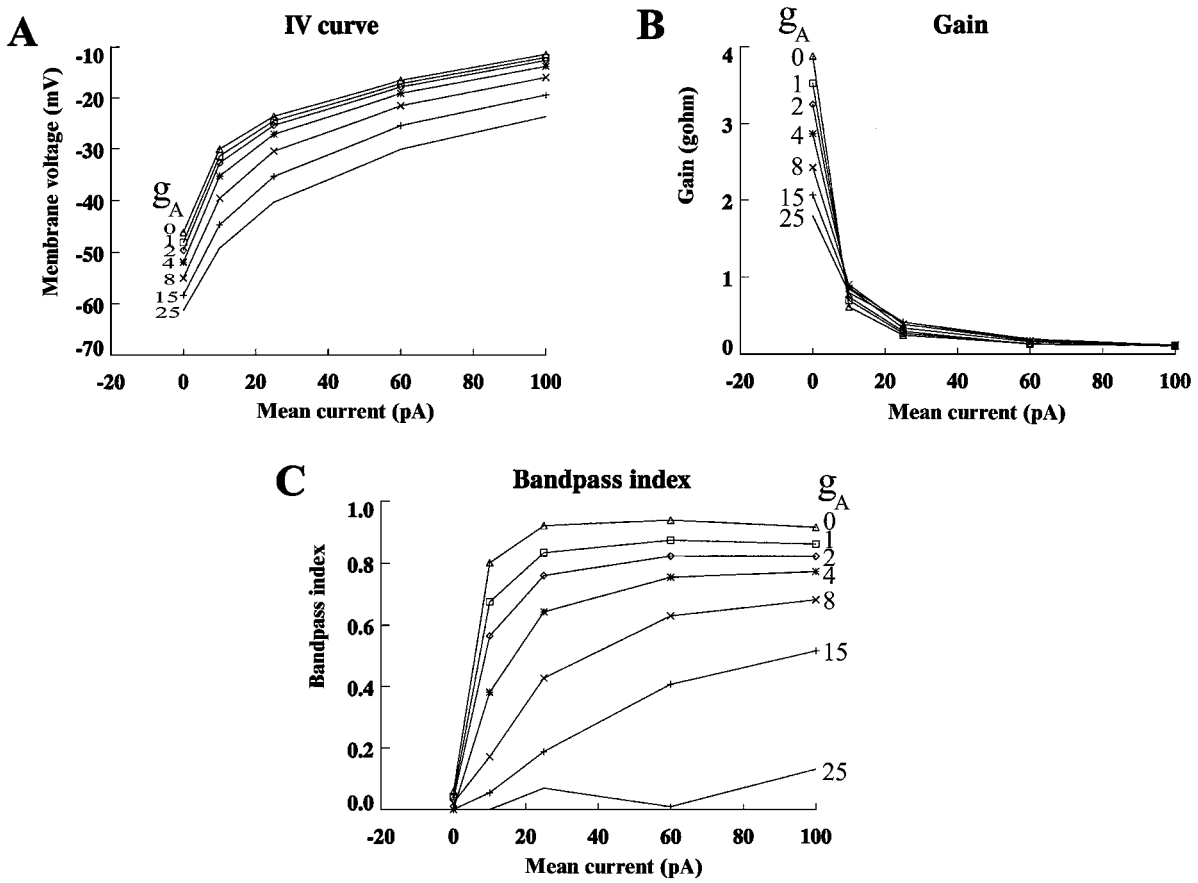

Figure 6. Effect of A-channel on I-V relation: Gain and bandpass behavior. Simulation of a set of model neurons with delayed-rectifier conductance G_{DR} of 5 nS and various A-channel conductances G_A. **A:** Membrane voltage as a function of mean injected current in a model neuron with G_{DR} equal to 5 nS, and G_A equal to 0 nS (triangle), 1 nS (square), 2 nS (diamond), 4 nS (∗), 8 nS (x), 15 nS (+), and 25 nS (no symbol). **B:** Gain as a function of mean input current for these model neurons (symbols are as in panel A). Note a progressive reduction of gain with increasing G_A. **C:** Bandpass indices as a function of mean current (values of G_A and symbols are as in panel A). Bandpass indices calculated as described in Results, one for each impulse response. (Impulse responses for G_A equal to 0, 4, and 15 nS are shown in Fig. 7). Note a progressive reduction of bandpass indices with increasing G_A.

Impulse responses were calculated approximately from the model neuron's response to a current impulse, with amplitude 500 pA and a very short duration of 0.01 ms (which approximates, in effect, a Dirac function), superimposed on the mean currents 0, 10, 15, 60, and 100 pA. Moreover, we previously demonstrated that model impulse responses obtained by this approximate impulse and those by m-sequence were indistinguishable from each other, but that only the latter method was feasible experimentally for signal-to-noise reasons (Mao et al., 1998). Thus, impulse responses are given by the model's response to this approximate impulse, divided by the "strength" of the impulse, 500 pA · 0.01 ms.

The overall adaptive behavior of the model neuron is summarized in Fig. 6. The A-channel causes a hyperpolarizing shift in the membrane potential at all mean injected currents (Fig. 6A; cf. Fig. 5E). Increases in A-channel conductance G_A reduce gain at resting potential and flatten the DC gain-mean current relation (Fig. 6B). Increases in G_A also reduce the shift to bandpass behavior of the model neuron, as is seen from the reduction of bandpass indices at all depolarizing mean currents (Fig. 6C). Indeed, as Fig. 7 shows, the delayed-rectifier alone causes an undershoot ($G_A = 0$). The A-channel ($G_A = 4$), via shunting, delays and reduces the incremental activation of the delayed-rectifier, thus reduces the depth of undershoots

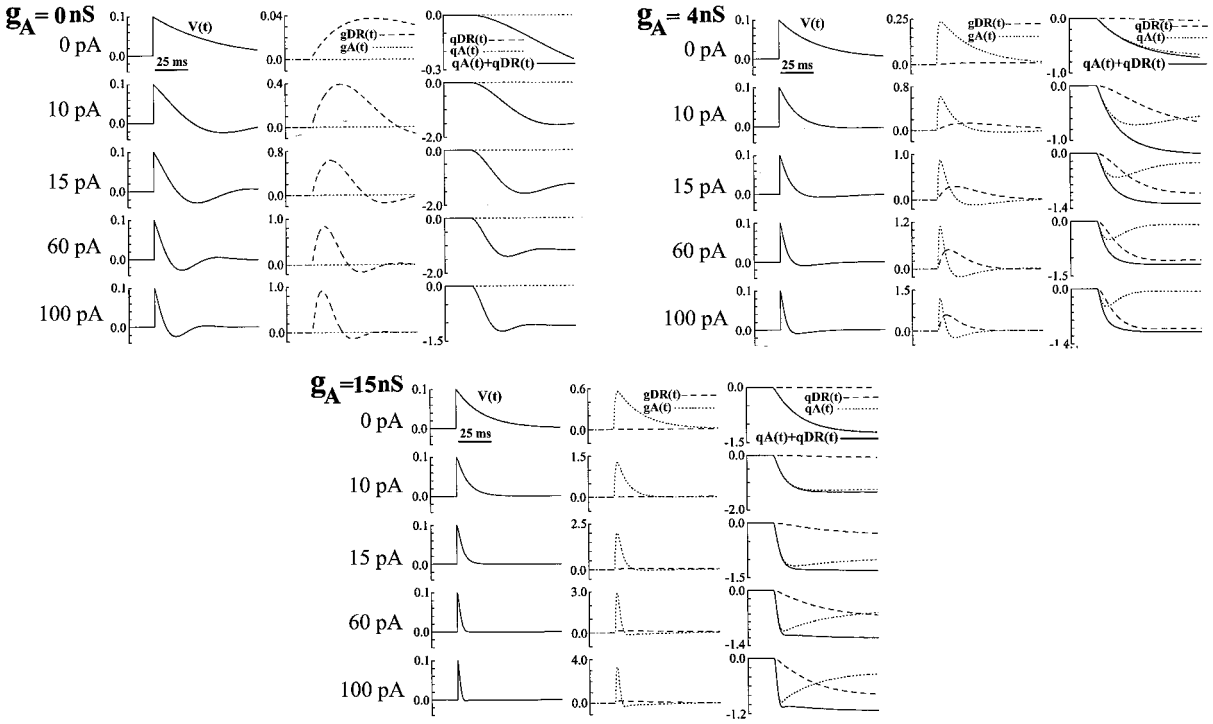

Figure 7. Interaction of the A-channel with the delayed-rectifier: Impulse responses. Impulse responses for model neurons with delayed-rectifier conductance G_{DR} equal to 5 nS and maximal A-channel conductances G_A of 0 nS , 4 nS , and 15 nS. For each value of G_A, impulse responses are shown for mean injected currents 0, 10, 15, 60, and 100 pA. For each mean injected current, impulse responses of 5 variables—$V(t)$, $g_A(t)$, $g_{DR}(t)$, $q_A(t)$, and $q_{DR}(t)$ (explained below)—are shown, as well as the sum of $q_A(t)$ and $q_{DR}(t)$. In all impulse responses, 0 is the steady-state level and positive (or negative) values are relative to this steady-state level. *First column*: $V(t)$: voltage; *second column*: $g_A(t)$: A-channel conductance (dotted line), $g_{DR}(t)$: delayed-rectifier conductance (dashed line); *third column*: $q_A(t)$: electrical charge through A-channel conductance (dotted line), $q_{DR}(t)$: electrical charge through delayed-rectifier conductance (dashed line), and the sum of the two (solid line). Values of $q_A(t)$ and $q_{DR}(t)$ are negative to represent the effect of potassium electrical flows on membrane potential. All impulse responses are calculated from the response of the model neuron to a very narrow current impulse, 500 pA · 0.01 ms, superimposed on the mean currents 0, 10, 15, 60, and 100 pA. All impulse responses were divided by the "strength" of the impulse, 500 pA · 0.01 ms. Note that the decay phase of the impulse response $V(t)$ largely reflects the decay phase of $q_A(t)$ and $q_{DR}(t)$, the sum of electrical charges through the A-channel and delayed-rectifier conductance. Note also the prominent undershoot for the model neuron with G_A of 0 nS and the near-absence of undershoot with G_A equal to 15 nS.

typically associated with the delayed-rectifier. With even higher G_A (15 nS), the undershoot disappears.

The effects of currents through K^+ channels must ultimately be reflected in the membrane potential. Under conditions of constant capacitance, electrical charge Q and voltage V are related by $Q = CV$, a relationship that also holds for increments in V and Q. To assess the relative contributions of A-channel and delayed-rectifier to impulse response, we calculated electrical charges through the A-channel and delayed-rectifier, $q_A(t)$ and $q_{DR}(t)$ in Fig. 7, by integrating currents through the two channels. Traces $q_A(t)$ and $q_{DR}(t)$ thus reflect contribution of each channel to impulse response $V(t)$. Note that $q_A(t)$ and $q_{DR}(t)$ assume negative values, reflecting the fact that the increments in K^+ conductance tend to bring membrane potential toward the K^+ reversal potential, which is more negative than the membrane potentials. Indeed, in Fig. 7, the decay phase of $q_A(t) + q_{DR}(t)$ (solid line) much resembles the decay phase of $V(t)$, although the match is not perfect, presumably due to the presence of other elements such as leakage conductances. By comparing the decay phases of $q_A(t)$, $q_{DR}(t)$ and $q_A(t) + q_{DR}(t)$, we assess the relative weights with which the currents through the two channels contribute to the impulse response $V(t)$. Thus, with an A-channel conductance G_A equal to 0 nS, all the electrical charges must flow through the delayed-rectifier (except for those through voltage-independent K^+ conductance and nonspecific leakage conductance), and the undershoot is evident for mean injected currents 10, 25, 60, and100 pA. With G_A equal to 4 nS, electrical charges flow through both

the delayed-rectifier and A-channel. An undershoot for mean injected currents 25, 60, 100 pA is still present but much shallower. Curves $g_A(t)$ and $g_{DR}(t)$ show that both conductances are open, but the relative effects of the two channels on impulse response are evident by comparing $q_A(t)$ and $q_{DR}(t)$. Since the A-channel activates much faster and is open for a much shorter time than the delayed-rectifier, the initial decay phase of impulse response $V(t)$ is dominated by the influence of A-channel. But the later phase of impulse response $V(t)$ is dominated by the delayed-rectifier, which, however, is less activated and more delayed due to the presence of the A-channel (cf. $V(t)$, $q_A(t)$, $q_{DR}(t)$ for G_A equal to 0 nS). With an even higher G_A (15 nS), the undershoot nearly disappears at all mean currents and A-channel dominates $V(t)$. In this regime, the effect of the delayed-rectifier on impulse response $V(t)$ is negligible.

Figure 8 shows how the shape and frequency range of transfer functions depend on A-channel conductance. With increasing A-channel conductance ($G_A = 0$, 4, and 15 nS), the frequency response broadens. Bandpass behavior is evident with G_A equal to 0 nS, is weakened with 4 nS, and essentially disappears with 15 nS. Comparable transfer functions obtained in bipolar cell recordings can be found in Mao et al. (1998).

4. Discussion

4.1. K^+ Channel Kinetics Shape the Dynamic Features of Neurons

Voltage-activated ion channels are functionally equivalent to elements of inductance or capacitance, depending on the conductance derivative $\frac{\partial g}{\partial V}$ and the reversal potential V_{rev}. An ion channel acts as an inductance if $(V - V_{rev})\frac{\partial g}{\partial V} > 0$ or as a capacitance if $(V - V_{rev})\frac{\partial g}{\partial V} < 0$ (Mauro et al., 1970; Detwiler et al., 1980; Koch, 1984). A delayed-rectifier at $V > V_{rev}$ behaves approximately like an inductive element, as an inductance does not allow a sudden change in current. In contrast, the A-channel, which activates instantaneously but transiently, approximates a capacitor. Generally, the transfer function of a circuit dominated by capacitance is lowpass (with current as input and voltage as output). Inductive elements are necessary for high-pass or bandpass transfer functions. Thus, the delayed-rectifier may cause bandpass behavior, but the A-channel cannot. Consistent with this view, a Ca^{++}-dependent K^+ current with a slow activation underlies a membrane

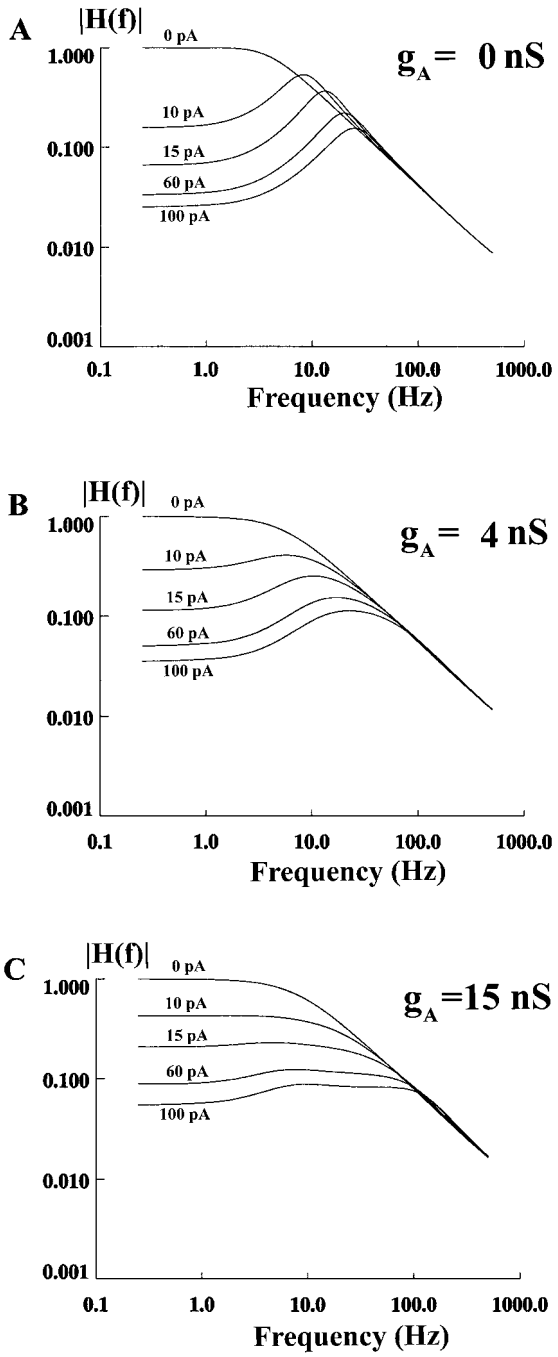

Figure 8. Interaction of the A-channel with the delayed-rectifier: Transfer functions. Transfer functions for model neurons with delayed-rectifier conductance G_{DR} equal to 5 nS and A channel conductances G_A equal to 0 nS (panel **A**), 4 nS (panel **B**), and 15 nS (panel **C**). In each set of transfer functions, curves from top down correspond to mean currents 0, 10, 15, 60, and 100 pA. Note that with increasing G_A, the range of frequency response expands and bandpass feature decreases. With $G_A = 15$ nS, the bandpass feature all but disappears.

oscillation in hair cells; and the A-channel is not involved (Lewis and Hudspeth, 1983). Conversely, TEA, which blocks the delayed-rectifier conductance, blocks membrane resonance in trigeminal root ganglion neurons (Puil et al., 1988).

A voltage-activated current may also be viewed as providing a feedback signal. Both the A-channel and the delayed-rectifier, selective for K^+, provide a negative feedback that accelerates the initial declining phase of the impulse responses (insets of Figs. 1A, 2A, and 4E). The delayed-rectifier by its sluggish nature introduces a time lag between its current and the voltage, a time lag that may be critical for the emergence of undershoot (Mao, 1997). In the frequency domain, the delayed-rectifier broadens the frequency response (via feedback), but it also causes bandpass behavior. In the presence of both conductances, the phase of the feedback signal that shapes the impulse responses is determined by the relative weight of each current, which in turns depends crucially on the temporal characteristics of the two channels. With the fast transient A-channel current, the impulse response begins to turn down with less delay. The A-channel thus speeds up the impulse response and removes the undershoot that is typically associated with the delayed-rectifier, in effect, by functioning as a shunt for the delayed-rectifier. In the frequency domain, the A-channel expands the frequency range and removes the bandpass features and, consequently, the frequency response becomes closer to that of an ideal amplifier (cf. Fig. 8A and C). Finally, it is noteworthy that, although the A-channel activates rapidly (as compared with the delayed-rectifier), the process still takes a finite amount of time. Thus, by the same principle as discussed above, the *activation process* of A-channel may cause undershoot and bandpass features of its own origin, a phenomenon that we indeed observed in our simulations. However, the undershoot and bandpass behavior associated with the A-channel activation is in a frequency range that is far above that in which the A-channel interacts with the delayed-rectifier. That this phenomenon was not observed in experiments may be attributed to the limitations in time resolution of the physiological recording system.

4.2. *K^+ Channels and Neural Information Processing*

Previous studies demonstrated that a delayed-rectifier K^+ channel suffices to account for the depolarization-induced dynamic changes in isolated bipolar cells—the reduction of gain, the shortening of the impulse response, and the bandpass behavior (Mao et al., 1998). This dynamic behavior bears strong similarity to observations in horizontal cells and ganglion cells during light adaptation of the intact retina (Tranchina et al., 1984; Purpura et al., 1990). However, the ranges of change in gain is narrower in our case, which indicates that bipolar cells' dynamic behavior cannot account for the entire dynamical change due to light adaptation in the retina (Mao et al., 1998). Some narrowing of the range of gains may be attributed to the presence of A-current, which, our simulations show, flattens gain-input relations (Fig. 6B), broadens frequency response, and reduces or preempts the bandpass behavior associated with the delayed-rectifier.

Subtypes of bipolar cells were suggested by studies in the retinas of other animals. In the white bass, a large type of bipolar cell possesses an A-channel current and two small types have an outward current of slower activation (Lasater, 1988). In goldfish retina, the A-channel and the AMPA receptor are co-localized to dendrites of OFF-bipolar cells (Yazulla and Studholme, 1999). Although it could be speculated that such subtypes would have distinct dynamics due to their different K^+ current components, we could not determine from our data whether dynamical subtypes exist in the tiger salamander. The general change in dynamics (gain and speed of response) was largely similar across all cells recorded. The resting potentials of isolated bipolar cells did not cluster into separate populations. The membrane potential at which K^+ current activates was relatively high (ca. -30 mV), and the voltage range at which the bandpass behavior occurs is relatively narrow (ca. -10 to -25 mV), which indicates that K^+ channel may act not only as a regulator of dynamics but also, in effect, as a mechanism to limit membrane potential range of the bipolar cells.

The functional role of K^+ channels may depend on their subcellular distribution. Since the majority of bipolar cells in our preparation lack axons, the A-channel and the delayed-rectifier currents we characterized must be on the soma or the dendrites. In bipolar and other retinal cells of other species, K^+ channels with particular kinetics have specific subcellular localization (Klumpp et al., 1995a, 1995b; Pinto and Klumpp, 1998). Somatodendritic K^+ channels in the bipolar cells may regulate synaptic transmission at the receptor-bipolar synapse, since synaptic gain is determined by the relative weights of the (glutamate-mediated) synaptic conductance and the

intrinsic (voltage-dependent) conductance (Falk, 1988; Tian and Slaughter, 1995). K^+ conductances with axonal distributions may also regulate synaptic transmission presynaptically, by negative-feedback control of Ca^{++} influx and neurotransmitter release.

In spiking neurons, the A-channel regulates spike-firing probability, spike width, and interspike intervals (Reyes et al., 1994; Zhou and Hablitz, 1996). A classical A-channel, found in the neural somata of a marine gastropod, prolongs interspike intervals (Connor and Stevens, 1971). In contrast, the type of A-channel that we characterized here narrows impulse responses and reduces undershoots and thus is similar to the A-channel that narrows action potentials and reduces interspike intervals in rat cortical layer 1 neurons (Zhou and Hablitz, 1996) and to the one that enhances repetitive firing at high frequencies in neurons of the avian cochlear nucleus (Reyes et al., 1994). The adaptive behavior caused by K^+-currents may also affect how neurons encode and process information along the spectrum of an integrator versus a coincidence detector (Konig et al., 1996). Coincidence detection is crucial in early central auditory processing, as sound localization requires resolving temporal differences in microsecond range. The mechanism for this appears to depend on the A-channel and AMPA receptors (Reyes et al., 1994; Trussell, 1997). The distinction between an integrator and a coincidence detector, however, may be a matter of degree: both modes of processing may be realized in a single neuron, with conversion from one mode to the other depending on the relative proportions of delayed-rectifier and A-type channels. Moreover, since the A-channel is subject to regulation by intracellular molecules, such as PKA (Jagger and Ashmore, 1999), the quantitative dynamics of neurons may also be subject to such regulation.

Acknowledgments

This investigation was supported by the NIH grant EY9314 to JDV. We thank Drs. Keith Purpura and Arlene Hirano for helpful discussions and advice, Dr. Rafael Yuste for the use of technical resources and support, and two anonymous reviewers for many helpful comments.

References

Attwell D, Werblin SF, Wilson M (1982) The properties of single cones isolated from the tiger salamander retina. J. Physiol. Lond. 328: 259–283.

Beech DJ, Barnes S (1989) Characterization of a voltage-gated K^+ channel that accelerates the rod response to dim light. Neuron 3: 573–581.

Connor JA, Stevens CF (1971) Prediction of repetitive firing behavior from voltage clamp data on an isolated neurone soma. J. Physiol. Lond. 213: 31–53.

Connor JA, Walter D, McKown R (1977) Neural repetitive firing: Modification of the Hodgkin-Huxley axon suggested by experimental results from crustacean axons. Biophys. J. 18: 81–102.

Detwiler PB, Hodgkin AL, McNaughton PA (1980) Temporal and spatial characteristics of the voltage response of rods in the retina of the snapping turtle. J. Physiol. Lond. 300: 213–250.

Falk G (1988) Signal transmission from rods to bipolar and horizontal cells: A synthesis. Prog. in Retinal Res. 8: 255–279.

Hare WA, Lowe JS, Owen G (1986) Morphology of physiologically identified bipolar cells in the retina of the tiger salamander, *ambystoma tigrinum*. J. Comp. Neurol. 252: 130–138.

Hille B (1967) The selective inhibition of delayed potassium currents in nerve by tetraethylammonium ion. J. Gen. Physiol. 50: 1287–1302.

Jagger DJ, Ashmore JF (1999) The fast activating potassium current, I(K,f), in guinea pig inner hair cells is regulated by protein kinase A. Neurosci. Letters 263: 145–148.

Kaneko A, Tachibana M (1985) A voltage-clamp analysis of membrane currents in solitary bipolar cells dissociated from *carassius auratus*. J. Physiol. Lond. 358: 131–152.

Klumpp DJ, Song EJ, Ito S, Sheng MH, Jan LY, Pinto LH (1995a) The shaker-like potassium channels of the mouse rod bipolar cell and their contributions to the membrane current. J. Neurosci. 15: 5004–5013.

Klumpp DJ, Song EJ, Pinto LH (1995b) Identification and localization of K+ channels in the mouse retina. Visual Neurosci. 12: 1177–1190.

Koch C (1984) Cable theory in neurons with active, linearized membranes. Biol. Cybernetics 50: 15–33.

König P, Engel AK, Singer W (1996) Integrator or coincidence detector? The role of the cortical neuron revisited. Trends in Neurosci. 19(4): 130–137.

Lasater EM (1988) Membrane currents of retinal bipolar cells in culture. J. Neurophysiol. 60: 1460–1480.

Laurent G (1990) Voltage-dependent non-linearities in the membrane of locust non-spiking local interneurons, and their significance for synaptic integration. J. Neurosci. 10: 2268–2280.

Lewis RS, Hudspeth AJ (1983)Voltage- and ion-dependent conductances in the solitary vertebrate hair cells. Nature 304: 538–541.

MacLeish PR, Barnstable CJ, Townes-Anderson E (1983) Use of monoclonal antibody as a substrate for mature neurons *in vitro*. Proc. Natl. Acad. Sci. USA 80: 7014–7018.

MacLeish PR, Schwartz EA, Tachibana M (1984) Control of the generator current in solitary rods of the *ambystoma tigrinum* retina. J. Physiol. Lond. 348: 645–664.

Mao B-Q (1997) The intrinsic dynamics of retinal bipolar cells and their ion channel mechanisms. Ph.D. dissertation, Graduate School of Medical Sciences of Cornell University, New York City.

Mao B-Q, MacLeish PR, Victor JD (1998) The intrinsic dynamics of retinal bipolar cells isolated from tiger salamander. Visual Neurosci. 15: 425–438.

Mauro A, Conti F, Dodge F, Schor R (1970) Subthreshold behavior and phenomenological impedance of the squid giant axon. J. Gen. Physiol. 55: 497–523.

Meves H, Pichon Y (1977) The effect of internal and external 4-aminopyridine on the potassium currents in intracellularly perfused squid giant axons. J. Physiol. Lond. 268: 511–532.

Owen WG, Torre V (1983) High-pass filtering of small signals by retinal rods. Biophys. J. 41: 325–339.

Perlman I, Sullivan JM, Normann RA (1993) Voltage- and time-dependent potassium conductances enhances the frequency response of horizontal cells in the turtle retina. Brain Res. 619: 89–97.

Pinto LH, Klumpp DJ (1998) Localization of potassium channels in the retina. Prog. in Retinal and Eye Res. 17: 207–230.

Press WH, Teukolsky SA, Vetterling WT, Flannery BP (1992) Numerical Recipes In C (2nd ed.). Cambridge University Press, New York.

Puil E, Gimbarevsky B, Spigelman I (1988) Primary involvement of K^+ conductance in membrane resonance of trigeminal root ganglion neurons. J. Neurophysiol. 59: 77–89.

Purpura K, Tranchina D, Kaplan E, Shapley RM (1990) Light adaptation in the primate retina: Analysis of changes in gain and dynamics of monkey retinal ganglion cells. Visual Neurosci. 4: 75–93.

Reyes AD, Rubel EW, Spain WJ (1994) Membrane properties underlying the firing of neurons in the avian cochlear nucleus. J. Neurosci. 14: 5352–5364.

Rudy B (1988) Diversity and ubiquity of K^+ channels. Neurosci. 25: 729–749.

Sutter EE (1987) A practical nonstochastic approach to nonlinear time-domain analysis. In: Marmarelis VZ, ed. Advanced Methods in Physiological System Modeling. University of Southern California Press, Los Angeles. Vol. 1, pp. 303–315.

Tessier-Lavigne M, Attwell D, Mobbs P, Wilson M (1988) Membrane currents in retinal bipolar cells of the axolotl. J. Gen. Physiol. 91: 49–72.

Thompson SH (1977) Three pharmacologically distinct potassium channels in molluscan neurones. J. Physiol. Lond. 265: 465–488.

Tian N, Slaughter MM (1995) Functional properties of a metabotropic glutamate receptor at dendritic synapses of on-bipolar cells in the amphibian retina. Visual Neurosci. 12: 755–765.

Tranchina D, Gordon J, Shapley RM (1984) Retinal light adaptation: Evidence for a feedback mechanism. Nature 310: 314–316.

Trussell LO (1997) Cellular mechanisms for preservation of timing in central auditory pathways. Curr. Opin. Neurobiol. 7: 487–492.

Victor JD (1992) Nonlinear system analysis in vision: Overview of kernel methods. In: Pinter RB, Nabet B, eds. Nonlinear Vision. CRC Press, Boca Raton. pp. 1–37.

Weckström M, Hardie RC, Laughlin SB (1991) Voltage-activated potassium channels in blowfly photoreceptors and their role in light adaptation. J. Physiol. Lond. 440: 635–657.

Yazulla S, Studholme KM (1999) Co-localization of Shaker A-type K+ channel (Kv1.4) and MAPA-glutamate receptor (GluR4) immunoreactivities to dendrites of OFF-bipolar cells of goldfish retina. J. Neurocytol. 28: 63–73.

Yeh JZ, Oxford GS, Wu CH, Narahashi T (1976) Dynamics of aminopyridine block of potassium channels in squid axon membrane. J. Gen. Physiol. 68: 519–535.

Zhou F-M, Hablitz JJ (1996) Layer I neurons of rat neocortex. I. Action potential and repetitive firing properties. J. Neurophysiol. 76: 651–667.